Recent Progress in Sciences

Science Publication Inc.

Research Article Open Access

Stochastic modeling of vehicle impact on reinforced concrete bridge piers: Assessment of structural reliability and resilience

Suman Roy *

Department of Civil and Environmental Engineering, Utah State University, Logan, Utah 84322, USA
* Correspondence: Suman Roy. email: sumanroy74@gmail.com

Received: June 23, 2025; Revised: August 15, 202x; Accepted: September 18, 2025; Published: September 30, 2025

Abstract

Vehicle impacts impose high strain-rate dynamic loads on reinforced concrete (RC) bridge piers, leading to complex material responses and an apparent strength increase, typically represented by the Dynamic Increase Factor (DIF). The initial collision often damages the concrete cover, redirecting load to the transverse reinforcement and altering the pier's axial and flexural performance. This study presents a streamlined mathematical model that evaluates damage severity, estimates failure probability, and calculates a reliability index for impacted piers. Compared to conventional probabilistic models, such as Normal, Log-normal, Weibull, Allen and Standardized Allen distributions, the proposed model yields slightly conservative but more consistent estimates of residual capacity, offering a more reliable assessment of structural performance under uncertainty. Validation through uncertainty analysis reveals a small deviation of ±4.3%, supporting the model's robustness. The results provide practical guidance for damage evaluation, re-strengthening strategies, and forensic investigations, making the model a reliable and cost-effective tool for engineers assessing RC bridge pier serviceability and resilience after high velocity vehicle impact.

Keywords RC pier, vehicle impact load, limit states, failure, predictive calibration method

1. Introduction

The growing volume and speed of vehicular traffic, along with the exposed and often vulnerable surfaces of reinforced concrete (RC) bridge piers, while particularly on overpasses, have raised significant concerns regarding their crashworthiness and structural reliability. Unlike seismic events, which have long influenced bridge design codes and safety protocols, vehicle impacts have historically received less emphasis, despite their proven risk. A comprehensive study of bridge failures from 1951 to 1988 revealed that approximately 53% were caused by impacts from heavy vehicles such as trucks, making vehicular collision the leading cause of bridge failure during that period, while earthquakes accounted for only about 1% [1]. In recent years, the rising frequency of high velocity vehicle collisions with RC pier has led to severe bridge damage and even collapses, drawing increasing global concern [2]. This stark contrast highlights a major oversight in current design and assessment practices. RC piers are especially susceptible due to their geometric configuration and exposed positioning, which increase the likelihood and severity of impact-related damage [3, 4]. High-speed collisions can result in a range of damage, from superficial cracking and concrete spalling to severe structural compromise or collapse. Alarmingly, many impacted piers remain in service without adequate health monitoring or damage assessment, increasing the risk of catastrophic failure if a secondary event, such as an earthquake takes place before repairs or reinforcements are made. This underscores the urgent need for detailed structural evaluations that consider sequential loading effects and the cumulative damage from multiple events. To ensure safe re-use or to determine the necessity of retrofitting or strengthening, comprehensive analyses must account for key factors such as pier geometry, material behavior, boundary conditions, and impact height, all of which exhibit inherent variability [5]. Given the complex interplay of factors like material properties, geometry, boundary conditions, and impact height, a more nuanced understanding of how RC piers perform under sequential loading is essential. Insightful structural evaluations and data-driven decisions on repair or retrofitting are needed to ensure long-term safety and resilience of bridge infrastructure in real-world impact scenarios. A deeper understanding of how RC bridge piers perform under these complex, real-world scenarios is essential for improving bridge safety, longevity,

and resilience against both isolated and compound hazards.

Recent studies have attempted to classify the serviceability of damaged RC bridge piers based on the severity of vehicular impact, ranging from slight to extensive damage [6]. While these efforts provide useful initial insights, they highlight the need for a more in-depth understanding of crash severity as a critical factor in determining whether a damaged pier can remain in service. Existing literature primarily focuses on identifying damage levels or enhancing structural survivability under impact [7], with limited emphasis on the dynamic response of piers under varying conditions. Some research works have explored the influence of parameters such as pier geometry, vehicle speed, impact mass, concrete compressive strength, and the tensile strength of reinforcement steel on pier reliability [8]. Despite recognition of the importance of risk-based design, current codes still often rely on overly simplified static approaches to model impact loads from vehicles, trains, or ships, frequently underestimating their effects for the sake of economic efficiency [9, 10]. To address these shortcomings, the present study introduces a mathematical model that captures the failure response of RC piers under high-velocity impacts by incorporating a strain-rate-dependent damage index. This model is evaluated against existing statistical models and used to conduct a parametric study, leading to a regression-based framework for predicting failure and assessing reliability through an improved reliability-based approach.

The incepted model has been compared with the widely used statistical models estimating pier impairment caused by high velocity semi-trailer impact. The shows its conservativeness whereas the statistical formalisms manifest close proximity that do not consider the uncertainty associated in estimating failure and corresponding reliability along with the sensitivity that warrants the structural resilience [11]. The model is further validated by uncertainty evaluation. This methodology is crucial for accurately estimating the reduced strength of in-service piers and guiding decisions on repair, retrofitting, or continued use. By addressing the performance of RC piers after impact and accounting for potential sequential hazards such as seismic events, this study aims to bridge existing knowledge gaps and support the development of more resilient and characterizing reliable bridge infrastructure [12].

This study offers a comprehensive investigation into the post-impact performance and residual structural capacity of reinforced concrete (RC) bridge piers, focusing on their behavior following vehicular collisions. A newly developed probabilistic model is introduced and critically evaluated against existing models to validate its predictive capability and practical applicability [13]. The aim is to establish a robust framework for assessing post-impact performance that extends beyond immediate damage characterization to encompass residual load-bearing capacity, an essential factor in post-event safety assessments and decision-making. The research emphasizes structural resilience, particularly under sudden, dynamic loading conditions, where understanding damage propagation and capacity retention is crucial.

The novelty of this study lies in the rigorous validation of the proposed model through a combination of stochastic analysis and scaled experimental testing using half-size RC bridge pier prototypes. These specimens are carefully designed to simulate the dynamic and structural characteristics of full-scale piers while enabling controlled observation of impact-induced behavior. Key aspects of the model's robustness are examined, including its ability to capture nonlinear damage progression, accurately correlate damage indices with residual strength, and predict failure probabilities under varying conditions. By normalizing performance metrics and comparing them across models, the study also facilitates a nuanced understanding of model reliability and trade-offs. Ultimately, this research contributes a standardized yet adaptable modeling framework capable of informing both design practice and post-impact assessment in critical infrastructure systems.

1) A detailed post impact performance of RC pier after experiencing high velocity single impact load and post impact pier performance in terms of reliability using various index methods. These indices are compared to come up with a cognitive and persuasive regression model to assess post impact performance warranted by high strain rate loading.
2) This study aims to develop a practical and comprehensive method for evaluating the severity of structural deterioration following an impact event and for accurately predicting the corresponding residual capacity of the structure. By focusing on the reduction in resilience caused by damage, the method seeks to provide a reliable assessment of a structure's remaining strength and performance potential. This approach integrates damage characterization with predictive modeling, offering a more informed basis for decision-making in post-impact inspections, repairs, and continued use.
3) This research study aims to facilitate detailed performance analysis and accurately capture the effects of uncertainty parameters, thereby enhancing the design capacity and refining the definition of failure domains. It offers a valuable tool for forensic structural engineers, enabling more reliable health assessments and evaluation of residual capacity in structures subjected to high velocity impact.

2. Vehicle impact load and failure of RC pier

The exposed reinforced concrete bridge column when experiences a vehicular, small to highly loaded truck, impact due the high momentum followed by shock which leads to the adequate damage to that pier. Reinforcing steel bar being a homogeneous and isotropic material, dissipates high energy and withstand substantial impact ([14, 15], low velocity and resilience coupler). This leads very significant to determine DIF.

In this study, vehicle weight (M) and impact velocity (V) of the semi-trailer are considered as 42.11 kips. (187.30 kN) and 100 ft/sec (30.48 m/sec) respectively [14]. In addition, due to high velocity impact, its damage is so detrimental that the bridge may undergo severe damage to completely collapse. The bridge pier having impacted, experiences high frontal shock causes an irreparable collapse. Although, some impacted bridge piers are relatively less damaged, which in turn, can be restrengthened and retrofitted into service [15].

2.1 Computation of damage

The load model used for the reliability analysis of a concrete pier subjected to vehicular impact is defined by the dynamic impact force exerted by the colliding vehicle. This dynamic force (I_{dyn}) is a function of the contact pressure (I_r) generated during impact, the geometric characteristics of the pier, and the duration of the impact event, as described in Equations 1 through 3 [3, 9]. In this analysis, the pier is assumed to have fixed-fixed boundary conditions, restrained against both displacement and rotation at the top and bottom ends, as illustrated in Figure 1. This configuration reflects a conservative assumption, capturing the most constrained response of the pier under short duration dynamic loading [11].

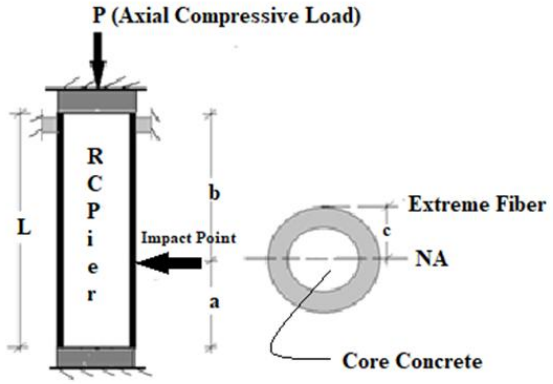

Figure 1 Impact location and geometry of RC bridge pier [11].

$$I_{dyn} = \frac{\int_{t_d-0.025}^{t_d+0.025} I_r \sin\left(\frac{\pi t_d^+}{t}\right) di}{0.05} \quad (1)$$

$$I_r = [(2 * 10^{-5}E) + 367.95] * \left[\frac{I * L^2}{(a * b^2 * c)}\right] \quad (2)$$

$$t = \sqrt{\frac{M}{k}} \quad (3)$$

where: I_{dyn} represents the dynamic impact force (also known as frontal shock) generated during a collision, I_r denotes the peak reflected pressure or overpressure resulting from the impact, t represents duration of the impact event, E signifies amount of kinetic energy absorbed by the impacted pier during the collision, I be moment of inertia of the pier's cross-section, which influences its resistance to bending, L is unrestrained (unsupported) length of the pier, a is the vertical distance from the base of the pier to the point where the impact occurs, b is vertical distance from the top of the pier to the impact point, c is the perpendicular distance from the neutral axis of the pier's cross-section to the farthest extreme fiber (often used in bending stress calculations), M is termed as vehicle weight involved in the collision, and k represents the stiffness of the vehicle's front structure, which affects how the vehicle deforms upon impact as illustrated in Figure 2.

Resistance models in reliability analyses are usually designed around material properties and geometric dimensions of the structural member under consideration. For impact analysis, the primary resisting mechanism of the pier is taken as its shear capacity.

As suggested in AASHTO LRFD [16] the design shear capacity of the reinforced concrete (RC) pier is determined using Equations 4 through 8 [11].

$$V_{N,design} = V_c + V_s \quad (4)$$

where: V_c is the shear strength carried by the concrete and V_s is the transverse shear capacity.

The shear strength, V_c, is computed as shown in Equation 5 [17].

$$V_c = \frac{6\sqrt{f_c'}}{\frac{\hat{s}}{D}} \sqrt{1 + \frac{N_{design}}{6\sqrt{f_c'}A_g}} (0.8A_g) \quad (5)$$

where: A_g represents the gross cross-sectional area of the concrete in the pier, $\hat{s}$ is the shear span, N_{design} is the design axial capacity of the pier and D is diameter of the pier cross-section.

The design axial capacity, N_{design} can be computed using Equation 6 [18].

$$N_{design} = 0.85(f_c') * (A_g - A_s) + \sigma_o * A_s \quad (6)$$

where: f_c' is the 28-day compressive strength of concrete, f_y is the first yield strength of main (longitudinal) reinforcing steel bar, σ_o indicates yield strength of reinforcing steel, and A_g and A_s represent the gross cross-sectional area of concrete and total cross-sectional area of longitudinal steel, respectively.

From the Equation 6, the design axial capacity of the pier has been determined as 1150 kips [4]. This is also furnished in Table 1.

Table 1 Materials and Geometric Properties of the representative RC Pier.

f'_c (ksi) (MPa)	f_y (ksi) (MPa)	A_g (in^2) (mm^2)	A_s (in^2) (cm^2)	A_{net} (in^2) (cm^2)	N_{design} (kips) (kN)
3 (20.68)	60 (413.68)	346.50 (2235.48)	4.70 (30.32)	341.80 (2205.16)	1150 (5115.45)

2.2 Evaluation of reduced capacity

Vehicle impacted and damaged residual column capacity can be computed introducing damage index (λ). Damaged column rating its severity, can be retrofitted for service. However, if the severity exceeds from highly damaged to collapse, the structural member shall no longer fulfill serviceability criteria. In this condition, the replacement of the structural member is inevitable. The assessment of damage level of the impacted pier has dealt a great concern. The damage of reinforced concrete material under impact load shall be identified by introducing some parameters, known as damage indices. To find the severity of the impacted damaged structure, damage index (λ) can play a significant role. Damage index, λ, can be assessed by the Equation 7 as shown in [19, 20].

$$\lambda = \frac{\mathrm{I_{dyn}}}{\mathrm{V_{dyn}}} \tag{7}$$

where: I_{dyn} is explained, and V_{dyn} expresses the dynamic shear due to high strain rate vehicle impact.

Damage index (λ) and residual strength (N_r) of the post damaged representative bridge pier is directly correlated, and is as shown in Equation 8 [19, 21].

$$\lambda = 1 - \frac{N_r}{N_{design}} \tag{8}$$

where: N_r is the residual strength of the damaged column after vehicular impact whereas N_{design} is the design axial load carrying capacity of the undamaged reinforced concrete bridge pier as stated in ACI.

By rearranging Equation 8, the residual strength of the damaged RC pier can be determined, as shown in Equation 9 [17].

$$N_r = (1 - \lambda) * N_{design} \tag{9}$$

where: f_c' is the 28-day compressive strength of concrete, σ_o is the yield strength of steel, and A_g and A_s are the gross cross-sectional area of concrete and total cross-sectional area of longitudinal steel, respectively.

Furthermore, the shear capacity offered by the transverse reinforcement, V_s is calculated using Equation 10.

$$V_s = \pi/2\, A_h \sigma_{yh}\, D'/s \tag{10}$$

where: A_h is the area of a single hoop or spiral, D' is the spiral or hoop diameter, s denotes the pitch of the helix, and σ_{yh} represents the yield stress of transverse steel (shear reinforcement).

The dynamic shear (V_{dyn}) and shear capacity of the pier (V_n) are correlated by the relationship shown in the Equation 11 [21].

$$V_{dyn} = V_n * (DIF) \tag{11}$$

where: DIF is the dynamic impact factor, and V_n is the shear capacity of the reinforced concrete (RC) pier with spirally arranged shear reinforcement.

The Dynamic Impact Factor (DIF) quantifies the increase in force experienced by a structure due to the dynamic nature of an impact, compared to a static load. The modulus of elasticity of the reinforcing steel bar at the strain hardening stage, E_P, is determined using Equation 9. However, DIF can be expressed in terms of quasi-static strain rate ($\acute{\varepsilon}$) as expressed in the Equation 15 via Equations 12 through 15. The variables used in Equation 12 through 15 are already explained earlier [4, 22, 23]

$$E_p = \sigma_P/\varepsilon_{eff} \tag{12}$$

$$\sigma_{dyn} = \left[1 + (\acute{\varepsilon}/C)^{1/P}\right] \cdot \left(\sigma_p + \beta E_p \varepsilon^{eff}\right) \tag{13}$$

$$\xi = 0.019 - 0.009\left(\sigma_{dyn}/60\right) \tag{14}$$

$$DIF = \left(\frac{\acute{\varepsilon}}{10^{-4}}\right)^{\xi} \tag{15}$$

where: $\acute{\varepsilon}$ is the strain rate considered as 5.4×10^{-4} s^{-1}, ξ is a constant which depends on the dynamic yield stress of steel at the strain hardening zone, σ_{dyn} is the dynamic yield stress of longitudinal (main) reinforcing steel, f_y is the initial yield stress, which is taken as 60 ksi (420 MPa) as per ASTM A706 for the yield stress at the elastic zone for grade 60 steel rebar, ε^{eff} is the equivalent plastic strain, taken as 0.72, E_p is the plastic hardening modulus, β is the hardening parameter which ranges from 0 to 1 and is taken as 0.5 in this study, and parameters C and P are the strain rate parameters as expressed in [12].

3. Load model and material properties of representative pier

3.1 Impact load application

To scrupulously evaluate the serviceability, structural integrity, and dynamic response of a circular RC bridge pier subjected to extreme loading, a detailed analysis was performed using a representative test prototype pier, as shown in Figure 2. The primary objective was to assess the pier's behavior during and immediately after a vehicular impact. Key areas of focus included deformation patterns, crack propagation, energy dissipation, and the residual load-carrying capacity of the column following the collision.

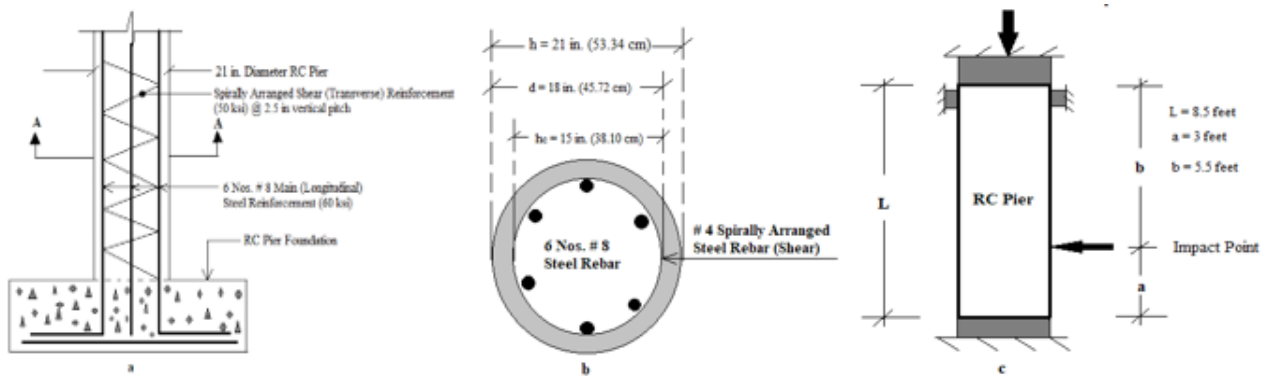

Figure 2 (a) Representative RC pier, (b) Section A-A, and (c) Load with end conditions. [11].

The test pier has been selected from a previous experimental study conducted by [24]. This report offers extensive experimental data, including geometry, material properties, reinforcement details, and impact testing procedures, all of which informed the current analytical and numerical investigations. Using a well-documented and validated specimen ensures alignment with established research, providing a solid foundation for evaluating the real-world performance of similar bridge piers under vehicular impact conditions.

3.2 Material properties

The test column has been prepared with a concrete grade of 3 ksi with a longitudinal (primary reinforcement) steel reinforcement of ASTM A706 [20] having grade of 60 ksi. From Figure 2, the detail of column cross-sections is well understood. The unrestrained length of the pier has been considered as 8.6 feet with varying cross-sections. From the top of the foundation level, up-to a height of 7 ft (section A-A) the column seems to be octagonal whereas the upper part is a rectangular (section B-B) with a length of 1ft.-6 in. The column has primary reinforcement of (6) #8 steel bars (main) throughout the foundation with a spiral shear reinforcement by #4 steel (grade of 36 ksi) bar @ 2-1/2 in pitch via helix formation throughout.

This research investigates how varying vehicular weights affect the performance of the test column GGSS-1 (24), which has been normalized to represent a traditional circular RC half-sized prototype bridge pier. A relationship has been developed to correlate different vehicle weights with both the λ and N_r of the column after impact. Additionally, the pier's geometry and boundary conditions used in the analysis are already illustrated in Figure 3.

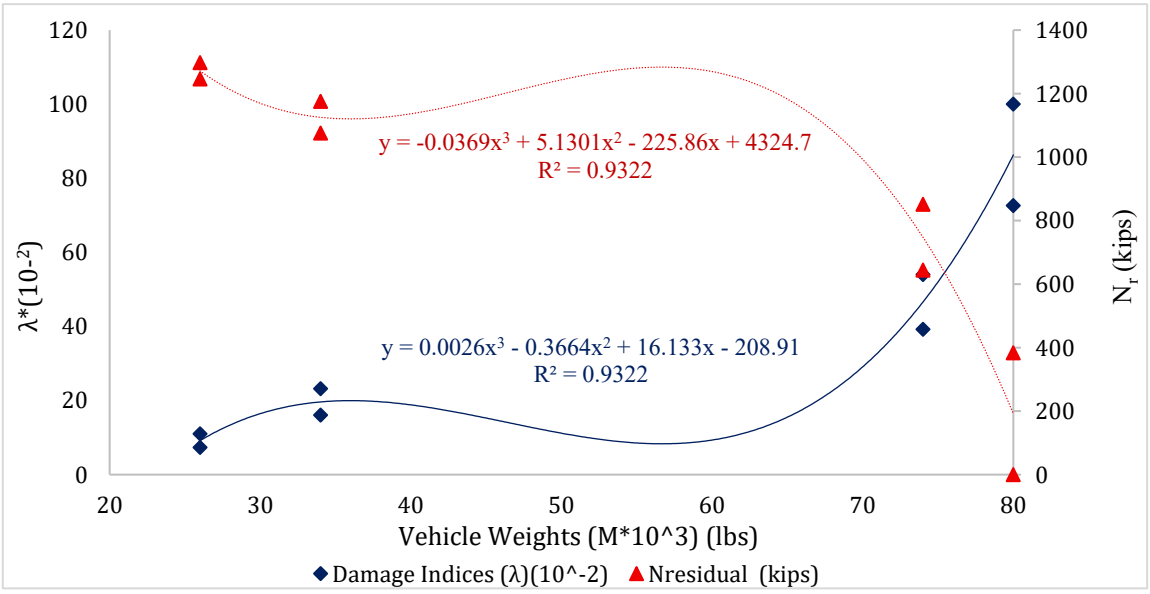

Figure 3 M with λ and N_r.

Figure 3 reveals a distinct and meaningful nonlinear relationship among vehicle weight (M), damage index (λ), and the normalized post-impact residual axial load (Nr). This relationship is most effectively modeled using a third-degree (cubic) polynomial regression, which captures the underlying complexities of the data without sacrificing interpretability. The decision to use a cubic model is grounded in both statistical performance and physical relevance: it achieves a high coefficient of determination (R^2 = 0.96 overall, and 0.932 for both M and λ), indicating that the model explains a substantial proportion of the variance in N_r.

The cubic polynomial is particularly well-suited for this application because it allows the model to express one

inflection point and up to two turning points endorses that align with the expected nonlinear behavior observed in real-world structural response data. For instance, as vehicle mass increases, its influence on damage and residual load may initially be marginal, then intensify beyond a certain threshold, and potentially plateau or even diminish under more extreme conditions due to material failure or energy dissipation mechanisms [21]. Such behavior cannot be adequately captured by linear or even quadratic models, which impose overly rigid assumptions about monotonicity or constant curvature.

On the other hand, higher-order polynomials, while capable of producing tighter statistical fits (i.e., higher R^2 values), often do so at the cost of model generalizability. They tend to introduce artificial oscillations between data points, an effect known as Runge's phenomenon leading to overfitting and decreased predictive robustness, especially outside the range of the observed data. This makes the cubic model a pragmatic middle ground. It is complex enough to reflect the nuanced interplay between impact conditions and structural response, yet restrained enough to maintain stability and physical interpretability.

The adequately fit model and theoretical justification behind the selection of model structure suggest that the cubic polynomial regression not only provides a statistically reliable representation but also encapsulates the physical interactions governing post-impact axial load behavior. This enhances confidence in its use for both analysis and predictive modeling in structural safety and resilience assessments.

Equations (16) and (17) present the derived mathematical expressions that define these correlations for the specific case of a high-velocity vehicular impact scenario applied to a half-scale reinforced concrete (RC) bridge pier specimen. These equations provide valuable insight into the complex structural behavior of the pier under dynamic loading conditions, and can be used to predict the residual capacity of the representative RC pier at specific impact scenario.

$$\lambda = 0.0026 * M^3 - 0.36 * M^2 + 16.13 * M - 208.91 \quad (16)$$

$$N_r = -0.036 * M^3 + 5.13 * M^2 - 225.86 * M - 4324.7 \quad (17)$$

where: λ, N_r, and M are already explained.

4. Prediction of probability of failure model

Probability of failure (P_f) in the damaged structures needs a rigorous study to predict the failure possibilities. Damage index (λ) provides a comprehensive understanding to assess the failure phenomenon. Any structural failure occurs when demand exceeds the capacity [25]. However, probability of failure in this research has been interpreted by the damage index (λ). Mathematically, probability of failure has been shown in Equation 18 [26].

$$P_f = \int_{-\infty}^{z\leq 0} g(x_i)x_i d_x = \int_{c}^{+\infty} \lambda(x_i)x_i \quad (18)$$

where: P_f is the probability of failure, λ represents damage index. In addition, $g(x)$ represents a performance or limit state function and x_i is a vector of all the random variables included in the limit state function.

From Equation 18, it is well understood that P_f is a function of λ. On the other hand, $(1 - \lambda)$ predicts the structural reliability. Determination of the P_f as a function of probability density function (PDF), shall be executed in performing the integration over the region of failure [27]. Estimated zone for predicting P_f can be easily identified from Figure 4.

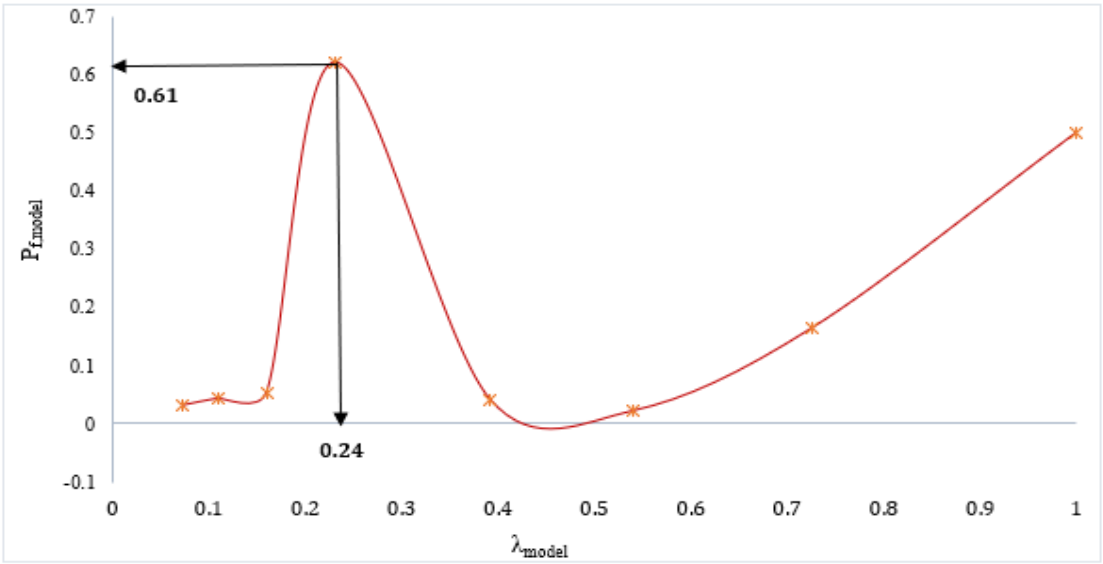

Figure 4 $P_{f,model}$ and λ_{model}.

Figure 4 reveals a distinct yet complex and quantifiable relationship between P_f and λ best described by a fifth-degree polynomial regression model. This model demonstrates a moderate fit, with an R^2 value of 0.63, indicating that it accounts for a significant portion of the observed variability. At approximately λ = 0.24, P_f reaches its peak value of around 0.62, forming a distinct plateau. This peak represents a critical transition point in the failure response, beyond which the system begins to exhibit recoiling behavior influenced by damping and oscillatory effects. Thus, λ = 0.24 addresses a pivotal threshold where the risk of failure has been captured highest.

Interestingly, within the range $0.41 \leq \lambda \leq 0.49$, P_f exhibits a temporary decline. This indicates that immediately after a high-velocity impact, the concrete briefly gains compressive strength, likely due to strain rate effects, which then diminishes as λ continues to increase. Despite ongoing damage accumulation, the failure probability growth rate stabilizes or slightly attenuates, likely due to energy dissipation mechanisms and structural resilience [21]. These post-peak dynamics underscore the role of the system's inherent responses in moderating failure progression. However, Figure 4 effectively illustrates the post-impact performance of piers under high-velocity, short-duration vehicle collisions, by precisely capturing the complex behavior under high strain rate loading [20].

4.1 Predicting probability of failure by Weibull

The Weibull distribution is a versatile statistical model commonly used in reliability engineering, failure analysis, and depicting survival strategies. It can accurately represent different types of failure rates; such as increasing, constant, or decreasing, by adjusting its shape parameter, making it ideal for modeling the life expectancy of structural elements and systems under various loading conditions. P_f for accidental damage has also been assessed by using Weibull method and introducing log-normal distribution as shown in [28]. Accordingly, P_f can be evaluated by using Equation 19.

$$P_f = \int_c^{+\infty} p(a) * \{1 - P_D(a)\} * da \qquad (19)$$

where: For the present study, $p(a)$ is i^{th} of damage index (λ_i) and $P_D(a)$ denotes the logarithmic distribution of damage index.

4.2 Predicting probability of failure by log-normal distribution

A log-normal distribution apprehends a positive-valued variable whose logarithm is normally distributed. It's useful for modeling things that grow multiplicatively, and tends to be skewed right with a long tail of larger values. By substituting the variables into Equation 19, the expression can be reformulated by using log-normal distribution in terms of λ, resulting in Equation 20 [27].

$$P_f = \int_c^{+\infty} \lambda(x) * \{1 - log(\lambda_i)\} * dx \qquad (20)$$

A comparative analysis between the failure probabilities predicted by the model described in Equation 19 and those derived from the Weibull distribution (Equation 20) reveals important distinctions in their predictive behavior and practical applications. The Weibull-based model (Equation 20) offers a more nuanced representation of failure patterns, particularly in its ability to describe the statistical distribution of damage across a range of severity levels. It captures the probabilistic evolution of failure more comprehensively, thereby enabling clearer delineation of failure zones and their parametric boundaries.

In contrast, the model defined by Equation 19 tends to adopt a more conservative side, producing failure probability estimates that can capture errors on the side of caution. This conservative bias can be advantageous in safety-critical contexts, where underestimating the risk of failure may have serious consequences. While potentially less precise in mapping gradual changes in damage progression, this model ensures a higher safety margin, making it particularly suitable for applications involving structural integrity under uncertain or variable loading conditions.

The Weibull model, on the other hand, often yields more liberal or optimistic predictions, reflecting its sensitivity to variations in material behavior and failure thresholds. While this can offer a more flexible and realistic depiction of failure probability under controlled conditions, it may underrepresent risk in scenarios involving high uncertainty or low fault tolerance.

Figure 5 visually contrasts the two approaches by depicting the probability of failure across various damage levels. The visualization highlights how the Weibull distribution captures a smoother, more continuous transition in failure likelihood, while the Equation 4 model shows a sharper and earlier onset of critical failure regions. This comparative depiction not only underscores the differing predictive philosophies of the two models but also offers valuable insight into their suitability for specific engineering applications, whether prioritizing reliability through conservatism or precision through statistical fidelity.

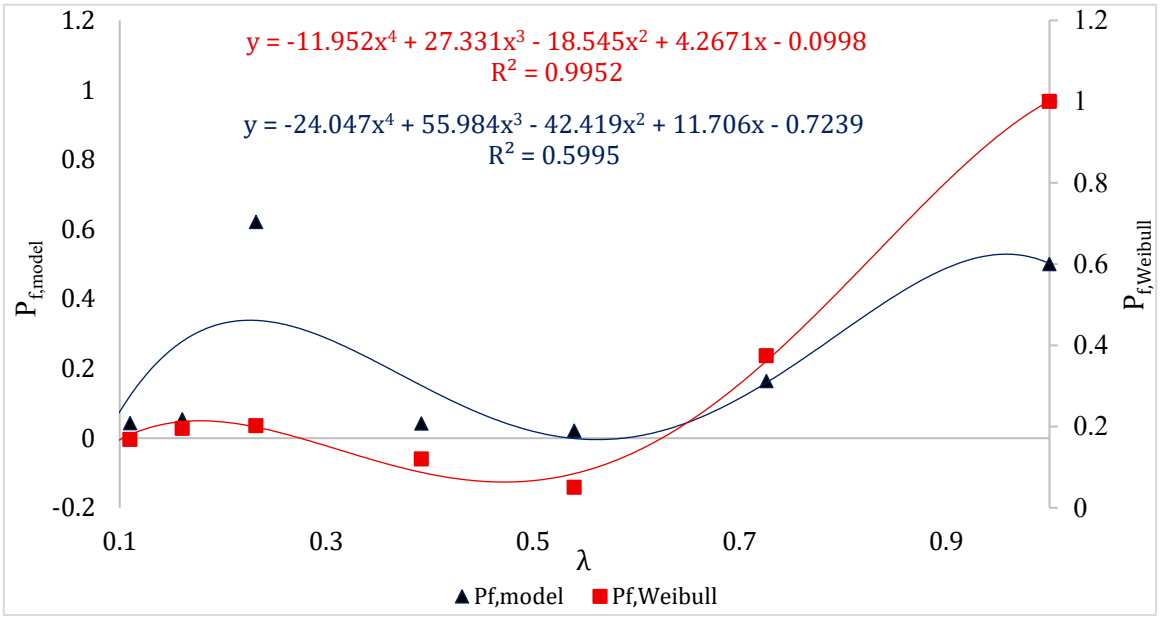

Figure 5 P_f and λ for Model and Weibull.

A comparative analysis has been conducted between the P_f models developed using the β formalism and Weibull distribution approaches, revealing notable distinctions between the two methodologies. The β-based model tends to produce conservative estimates, consistent with previous observations, indicating a cautious prediction of failure probability. In contrast, the Weibull model exhibits slight fluctuations or variability in its predictions, reflecting its sensitivity to data nuances.

Both models establish relationships between the P_f and the parameter λ, as described in Equations 21 and 22. Equation 21, representing the β model, yields a moderate coefficient of determination (R^2 = 0.6), indicating a conservative yet reasonably and accurately fit to the observed data. In contrast, Equation 22, based on the Weibull formalism, exhibits an exceptionally high R^2 value of 0.99, suggesting an almost overfitting the data. However, this apparent precision is potentially misleading, as it fails to adequately represent the underlying risk, particularly within the regions characterized by high uncertainty or large negative gradients, and obscuring critical failure domain and post impacting behavior in practical implementations.

In addition, the stark contrast in R^2 values, highlighting a value of 0.99, demonstrates the Weibull model's stronger ability to capture the underlying relationship between P_f and the corresponding λ. This indicates its superior precision in modeling observed behavior. In contrast, the β model, though more conservative, may be preferable in safety-critical applications where underprediction of failure could have serious consequences having windows to move with data precision back and forth. These findings underscore the inherent trade-off between precision and robustness, while the Weibull model offers closer alignment with data trends, its tendency to produce negative values in certain regions may undermine its practical validity. The β_{model}, despite potentially lower accuracy, provides a more stable and cautious estimate depicts an essential attribute in predicting the risk-averse scenarios.

$$P_{f,model} = -11.52(\lambda^4) + 27.11(\lambda^3) - 18.54(\lambda^2) + 4.26(\lambda) - 0.09 \quad (21)$$

$$P_{f,Weibull} = -24.05(\lambda^4) + 55.98(\lambda^3) - 42.52(\lambda^2) + 11.70(\lambda) - 0.72 \quad (22)$$

where: P_f and λ are already explained.

5. Assessment of reliability

The damage and probability of failure have been well correlated, and failure due to dynamic intensity will predicted. However, this needs an intensive parametric study prior to be commended Reliability analyses are performed to evaluate the performance of structures in real-world conditions with uncertain loadings and structural details. Simple structural analysis will show if a structure will or will not fail under precise conditions; in cases where the structural demand or resistance is non-deterministic, a reliability analysis is instead used to determine the likelihood of failure, [11].

Reliability of any structural failure phenomenon can be figured out by introducing reliability index (β), which is the inverse of the variation of probability of failure (P_f), and hence represented in Equation 23 [20].

$$\beta = -\Phi^{-1}(P_f) \quad (23)$$

where: Φ^{-1} is the inverse of the tail probability function of the standard normal distribution, P_f and β are already explained.

The P_f and corresponding β are essential metrics in bridge engineering that quantify the likelihood of structural failure and provide a standardized measure of safety, respectively. Nowak's work [25] is foundational in calibrating these values specifically for

bridges, establishing consistent and practical guidelines that engineers worldwide rely on [21]. His standardization enables uniform safety assessments across different bridge designs and loading conditions, bridging the gap between theoretical reliability concepts and real-world applications. Moreover, predictive models for reliability indices that closely align with Nowak's standards confirm their accuracy and usefulness, allowing engineers to confidently evaluate and enhance bridge safety without always resorting to extensive physical testing. This approach ultimately supports safer bridge designs, informed maintenance prioritization, and robust engineering codes, ensuring public safety and infrastructure resilience.

5.1 Reliability prediction by normalization

Reliability assessment of the failure criteria can be well anticipated by normalizing the failure zones. Hence, cumulative distribution function (CDF), Φ(z), can be followed by with the feasible uncertainty conditions as shown in Equation 24 [26].

$$\Phi(z) = \frac{1}{\sqrt{2\pi}} \int_{-\infty}^{z \le 0} \exp\left(-\frac{z^2}{2}\right) dz \qquad (24)$$

where: Φ is CDF of the standard normal random variable.

5.2 Reliability prediction by Allen Method

The design criteria in the Canadian Code of practice (CSA-S6-88) are based on a reliability index of 3.5 for a reference period of 50 years, whereas β referred for period of one year. This period has been chosen as a more suitable for bridge evaluation. For bridge elements the β for one year, corresponding to a βof 3.5 for 50 years has been shown. However, β resulting 3.5 for elements carrying dead load only and 4.0 for elements carrying traffic load only [25]. Notionally, P_f in respect of β has been utilized for bridge calibration. Model predicting β has been compared with the results derived via using Allen [29] and Nowak [25].

5.2.1 Standardized Reliability Indices for the Bridge Calibration

There is a need for β to be standardized to characterize the bridge calibration considering different parameters [29]. However, P_f in bridge based on different perspectives are taken into account for the standardization. In this approach, β determined is based on a one-year time interval for all traffic categories except for permit controlled and supervised vehicles, where β is based on a single passage β_{Allen} is standardized and shown in Equation 25 [29].

$$\beta_{Allen} = 3.5 - [\Delta_E + \Delta_S + \Delta_I + \Delta_{PC}] \geq 2.0 \qquad (25)$$

where: Δ_E is considered as 0.25, Δ_S is 0.25, Δ_I is 0.25, and lastly Δ_{PC} as 0.6, that yields a more conservative standardized value for $\beta_{standardized,\ Allen}$ as 2.15.

5.2.2 Comparison of Reliability Indices

In this research, a model has been developed to predict β and corresponding P_f to assess better structural stability and or vice-versa before recommending the structure in service. Nowak has recommended β (β_{Nowak}) [25] in terms of P_f. Here, β_{Nowak} has been standardized as a reference, and compared with the model for the sake of prediction. P_f has been related with β determined from various models as shown in Figure 6.

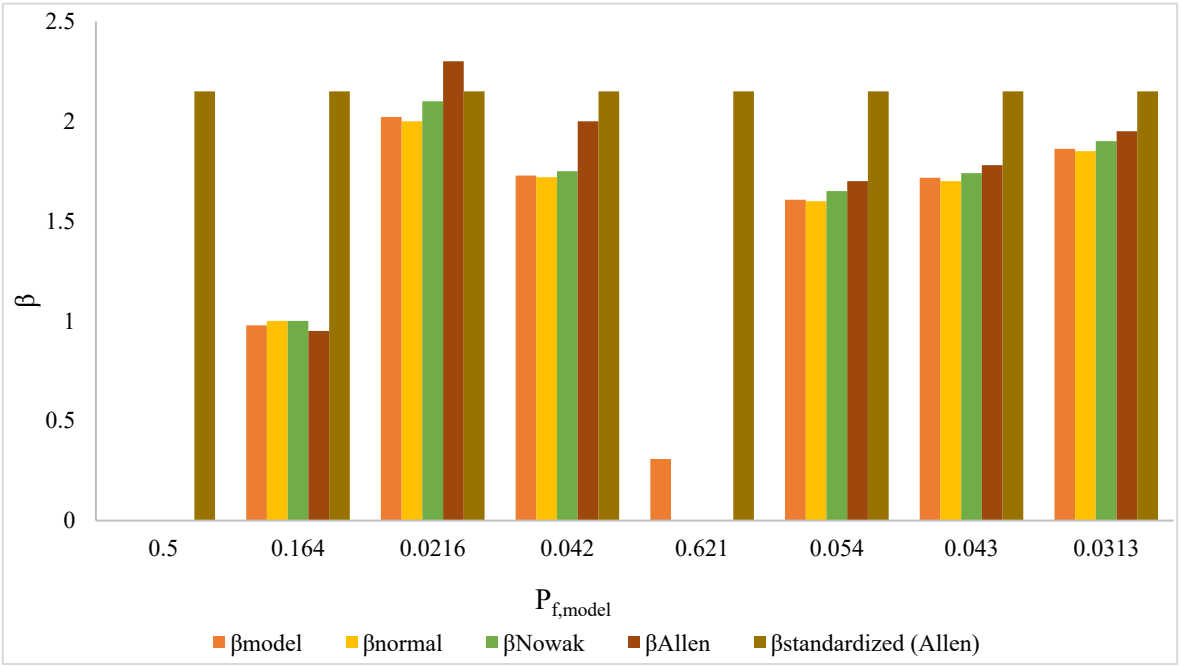

Figure 6 P_f and various β.

The estimated P_f was initially predicted using the Weibull distribution, a versatile and widely recognized model in reliability analysis due to its ability to represent a broad range of failure behaviors, from early-life failures to wear-out phases. Its shape and scale parameters allow flexibility in modeling structural response under different stress conditions, particularly in high-strain-rate scenarios such as vehicular impacts. Given the nature of RC pier response under dynamic loading, the Weibull distribution offers a more realistic representation of progressive failure mechanisms compared to more rigid models.

To evaluate the robustness and consistency of the failure predictions, β derived from the Weibull model were compared against those obtained from the proposed analytical model and the commonly used Normal distribution. Although the Normal distribution remains a staple in engineering applications due to its mathematical simplicity, it assumes symmetry and constant variance, which may not accurately reflect the stochastic nature of impact-induced damage. The comparative analysis, as delineated in Figure 7, highlights critical differences in the estimation of failure probability and structural reliability across these models. The results not only validate the proposed model's conservativeness but consistently predict and emphasize the importance of choosing an appropriate distribution for reliability assessment in dynamic impact scenarios. This integrated comparison provides a more comprehensive understanding of failure behavior, enhancing confidence in the model's application for post-impact evaluations, damage assessment, restrengthening along with the design calibrations.

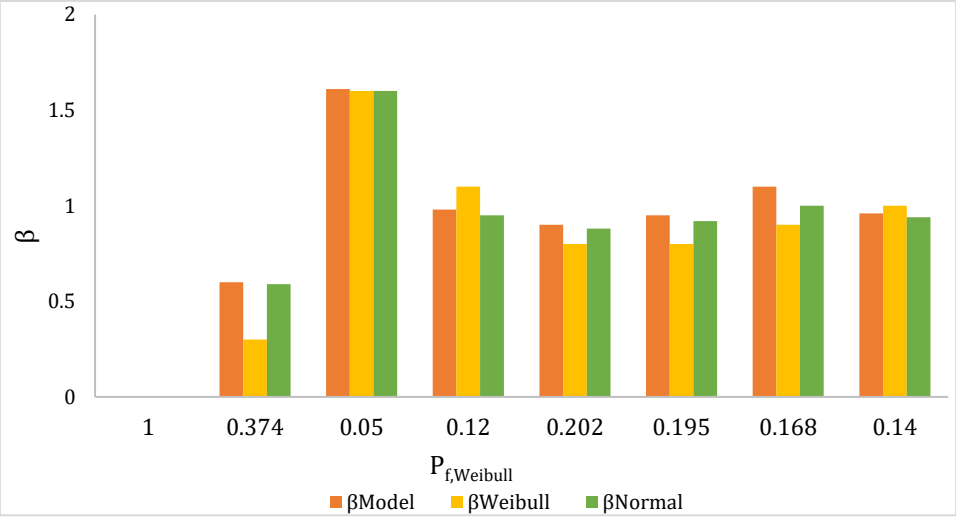

Figure 7 Weibull failure and various β.

In addition, P_f and the corresponding β derived from various computational models have been examined through a parametric study to identify regions within the system that are more prone to failure. By systematically varying input parameters and observing their impact on P_f and β, the analysis helps address out potential failure zones and quantify their reliability levels. This approach provides valuable insight into system behavior under different conditions, guiding decision-making for safer and improved design. The results are visually presented in Figure 8.

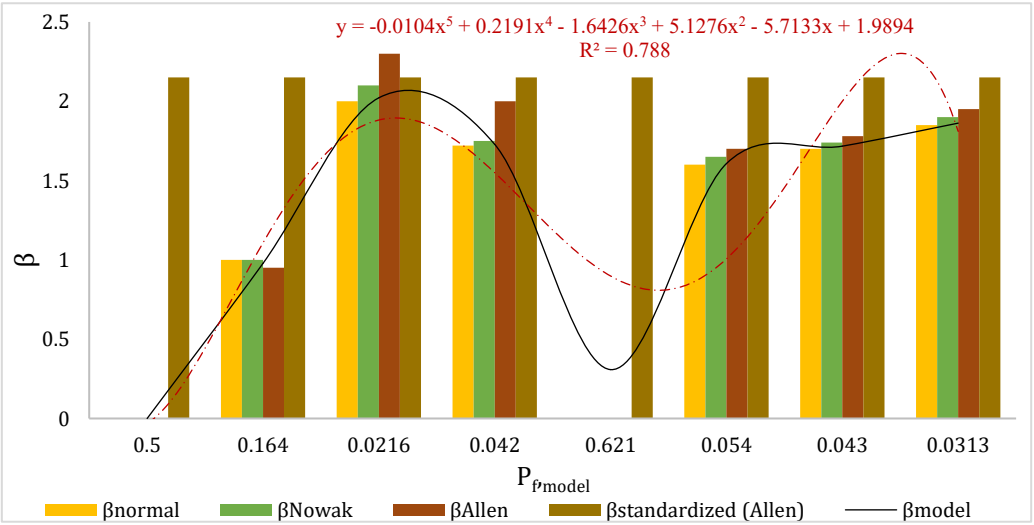

Figure 8 Failure prediction with the various β.

Capturing results from Figure 7, trending pattern of model has been formalized to Equation 26, with decently increased and tight R^2 value of 0.79.

$$\beta_{model} = -0.01 * p_f^5 + 0.22 * p_f^4 - 1.64 * p_f^3 + 5.12 * p_f^2 - 5.71 * p_f + 2.0 \quad (26)$$

where: β_{model} addresses reliability index of model and P_f is the corresponding probability of failure for the specific predictive model.

Figure 8 can capture the failure zone and its reliability from its determined from, and failure envelop predicting the feasible reliability zone.

Additionally, a whisker plot as a key analytical tool to evaluate and compare the reliability indices of different models, as derived from various statistical failure formalisms has been employed. The whisker plot effectively captures the spread, central tendency, and variability of the data, enabling a clear visualization of how each model performs under uncertainty. By displaying the median, interquartile range (IQR), and potential outliers, the plot provides critical insights into the robustness and consistency of each model's predictions, facilitating a deeper understanding of their relative reliability.

A whisker plot, or box-and-whisker plot as shown, represents a statistical diagram that visually summarizes the distribution of a dataset which has been furnished in Figure 9. It displays the median, IQR, and overall spread of the data, while also identifying potential outliers. The box represents the middle 50% of values (from the first quartile to the third quartile), with a line indicating the median. The 'whiskers' extend to the minimum and maximum values within 1.5 times the IQR, and any data points beyond this range are marked as outliers. This plot is especially useful for comparing variability and detecting skewness or anomalies across multiple data groups. This contributes to an insightful understanding that facilitates bridging the gap between the developed mathematical model and other established models.

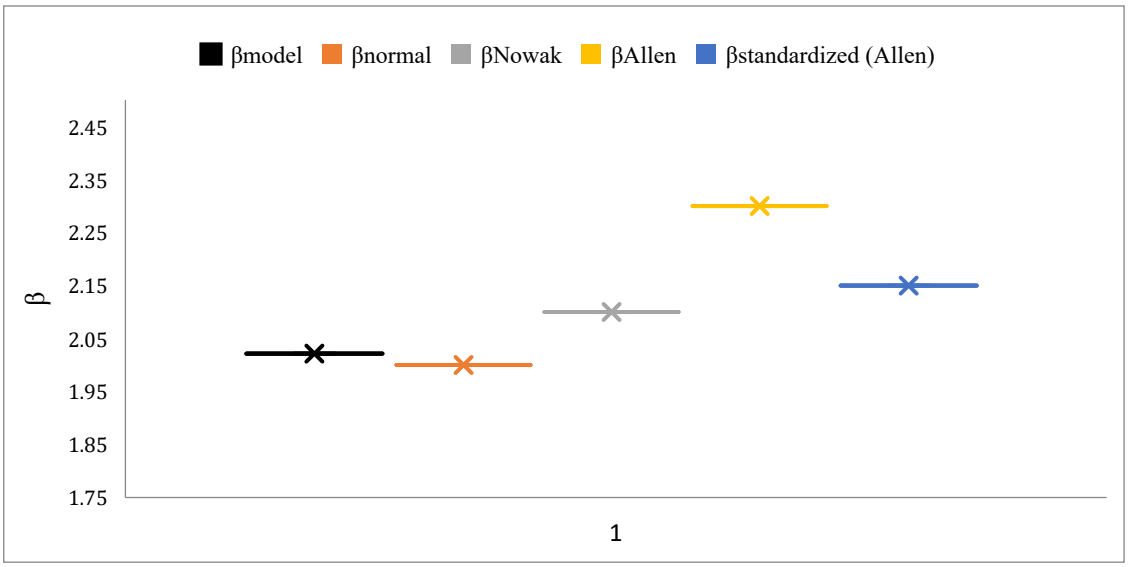

Figure 9 Failure prediction via various β.

6. Reduction in reliability index

A comparative analysis of Figures 6 through 9 indicates that the developed model for estimating the β demonstrates conservative behavior, producing values slightly higher than those predicted by the failure model based on a log-normal distribution. To further assess and visualize the performance of these models, Figure 9 employs a whisker plot, a robust statistical tool that highlights the distribution characteristics of β across multiple failure formalisms. This plot provides a detailed view of central tendency, spread, and potential outliers, facilitating a nuanced comparison of model behavior under uncertainty.

The use of percent difference in β values (p) serves as a critical parametric indicator for evaluating post-impact performance, demonstrating that the proposed model consistently holds a strong and stable position relative to the established statistical benchmarks. This metric is essential in statistical analysis because it quantifies the relative deviation between predicted and reference values, enabling normalized and meaningful comparisons across different models or datasets. By providing a clear measure of model accuracy and stability, especially under varying conditions, percent difference helps validate the reliability of predictions. Consequently, the β value derived from the proposed model has been substantiated as a reliable control benchmark, and hence corroborated as a control parameter and standardized metric.

This conclusion is further supported by sensitivity studies conducted by [11], which confirms the model's robustness across a range of impact scenarios. Additionally, the percent difference data summarized in Table 2 strengthens this assessment by offering a quantifiable evaluation of the model's reliability performance, particularly in the demanding context of short duration high-velocity truck collisions.

Table 2 Percent difference in β.

β	Magnitude	% Difference (p)	Standard deviation (SD)
β_{model} (Control)	2.03	0	
β_{normal}	1.99	2.01	4.49
β_{Nowak}	2.1	3.33	
$\beta_{standardized(Allen)}$	2.14	5.14	
β_{Allen}	2.3	11.74	

Table 2 offers a detailed examination of how the β varies in relation to the percent difference of itself (p), effectively illustrating the model's response under different probabilistic scenarios. This comparison provides not only a quantitative measure of performance but also insight into how well the model captures the underlying uncertainty in structural response. A key observation from the table is the computed standard deviation (SD) of β, which is found to be 4.49. This relatively low SD indicates a narrow spread of β values, suggesting that the model outputs are consistent and not heavily influenced by outliers or extreme variations. Such statistical stability reinforces the reliability of the model when applied across a wide range of failure probabilities.

To further enhance the interpretability of these findings, the relationship between β and p has been visualized in Figure 8. This plot offers a graphical representation of the trends observed in Table 2, allowing for more intuitive and immediate comprehension of how the β behaves across different probability thresholds. By capturing this data visually, Figure 8 reveals the overall shape and consistency of the β distribution, highlighting areas of both stability and transition. Conjointly, Table 2 and Figure 10 complement each other by combining stochastic precision with visual clarity, reinforcing the conclusion that the proposed model performs reliably and maintains predictive coherence under varying levels of probabilistic demand.

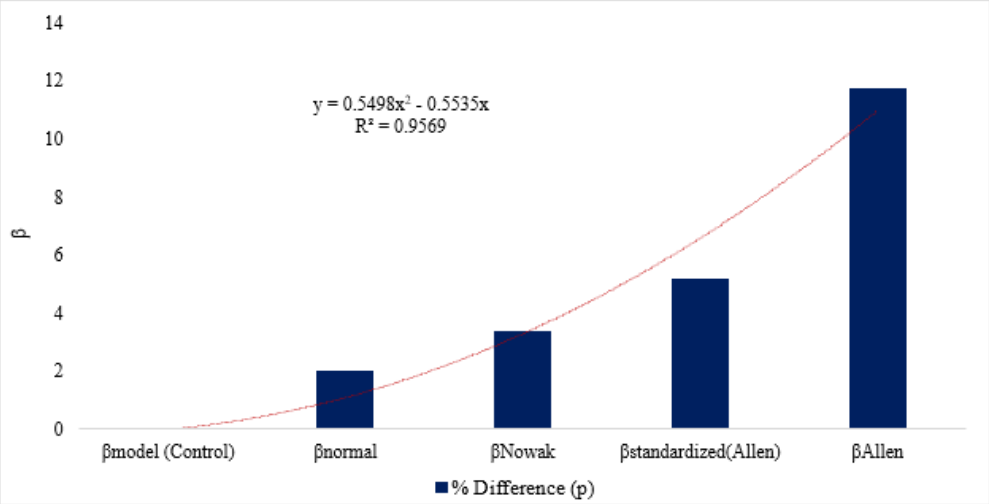

Figure10 β for various p.

From Figure 10, a holistic relationship between the β and p using different probabilistic models can be interpreted and formalized, as described by Equation 27. This equation provides a mathematical foundation for understanding how variations in various β from β_{model} influence the corresponding values of p, enabling a more comprehensive interpretation of the model's probabilistic behavior tailored due to percent variation. The visual trend observed in Figures 8 and 9 align closely with the theoretical relationship expressed in Equation 27, further validating the model's consistency and its applicability in reliability-based assessments.

$$\beta = 0.55 * (p^2 - p) \quad (27)$$

where: β and p are already explained.

Equation 27 has been derived from a smooth second-degree polynomial fit, as illustrated in Figure 9, with a high coefficient of determination (R^2) value of 0.96. This strong correlation indicates that the polynomial model accurately captures the trend between the various β and the p, validating the quality and consistency of the data. The close fit not only reinforces the functional relationship between β and p but also enhances confidence in using this model for predictive reliability analysis to precisely trigger the failure domain.

This polynomial correlation proffers a deeper conceptual understanding of the interrelationship between the β and the p as illustrated, particularly in the context of structural failure assessment. As β increases, the associated P_f obviously decreases, though the trend, as observed in the polynomial curve suggests a gradual

and nonlinear transition rather than a sharp drop. This smooth curvature reflects a nuanced, interpretable pattern in which the change in failure probability occurs progressively with increases in reliability, rather than abruptly. Such behavior is especially valuable when assessing structural performance under varying levels of uncertainty and impact severity.

The practicality of this polynomial fit lie in its ability to accurately represent this inverse relationship while maintaining a high degree of statistical integrity. The minimal standard deviation (SD) of β values, as shown in Table 2, supports the consistency of the model and indicates a low level of variability in its predictive outputs. Coupled with a high coefficient of determination (R^2 = 0.96), the model demonstrates strong predictive reliability and an excellent fit to the data. Altogether, the tight correlation, low variability, and smooth trend provide a robust and improved framework for correlating reliability and failure probability, an essential component for reliable failure risk evaluation in high-impact scenarios such as critical infrastructure assessments at high speed vehicular collisions.

6.1 Uncertainty prediction

Uncertainty prediction is the process of quantifying the degree of confidence or doubt in a model's output, which plays a pivotal role in statistical assessments and decision-making systems. Rather than offering a single deterministic prediction, models that incorporate uncertainty provide a range or distribution that reflects possible variation in outcomes. This is particularly critical in fields such as structural engineering reliability where high-stakes decisions depend not only on the predicted values but also on how reliable those predictions are. By identifying regions of high uncertainty, analysts can flag results that require cautious interpretation, reduce overconfidence in flawed predictions, and improve the credibility and safety of automated systems. However, this seemingly complex mathematical analysis warrants deeper scrutiny.

The precise estimation of overall uncertainty ($\bar{U}$) is often achieved through sensitivity analysis, using mathematical tools such as partial derivatives within established frameworks like the β-p model. As described by Holman (J.P.), Equation 10 demonstrates how $\bar{U}$ can be derived by considering small changes in each independent variable x_i affect and control the output. This approach allows for the decomposition of total uncertainty into individual contributions ($\bar{U}_i$ where *i = 1, 2, 3, ……., n*), as outlined in Equation 12. By isolating these components, practitioners gain insight into which variables most influence the model's uncertainty, helping prioritize data collection, refine models, and reduce error propagation. This not only improves the model's predictive accuracy illustrate risk but strengthening its interpretability and operational resilience [19, 30] as shown in Equation 28.

$$\bar{U} = \pm\left[\begin{matrix}\left\{\left(\frac{\partial\beta}{\partial x_1}\right) * \bar{U}_1\right\}^2 + \left\{\left(\frac{\partial\beta}{\partial x_2}\right) * \bar{U}_2\right\}^2 \\ + - - - \mp\left\{\left(\frac{\partial\beta}{\partial x_n}\right) * \bar{U}_n\right\}^2\end{matrix}\right]^{\frac{1}{2}} \quad (28)$$

where: $\bar{U}$ is the overall uncertainty, $\bar{U}_i$ be the uncertainty associated in the individual variable, and $\partial\beta/\partial x_i$ represents the partial derivative of β with respect to individual variables x_i, *where i = 1, 2, 3, ……., to n.*

In order to simplify the uncertainty analysis, the model has been reduced to focus on two primary variables: β, the dependent variable, and p, the independent variable. This reduction not only carries out the analysis more tractable but also centers attention on the most influential parameters affecting system performance. Within this reduced framework, Equation 10 has been normalized to express the total uncertainty ($\bar{U}$) in terms of just these two variables. By isolating β and p, the model minimizes complexity while retaining the ability to capture the dominant sources of variability that improves the model.

To estimate the uncertainty specifically associated with p, the analysis utilizes a conservative mean value, denoted as p_m, drawn from empirical data presented in Table 2. Using a mean value ensures stability in the uncertainty estimation process, particularly when data variability is limited or when worst-case scenarios must be avoided in sensitive applications.

To further streamline the calculation of uncertainty, Equation 12 is reformulated by reducing variables, resulting in Equation 13 as described by Holman (J.P.). This approach enables the propagation of uncertainty across multiple variables by evaluating how infinitesimal changes in each input contribute to the overall variation in the output. Once the independent parameters are normalized, partial derivatives can be used to assess the sensitivity of the dependent variable with respect to each input, one at a time, while holding the others constant. Despite the stepwise nature of partial differentiation, this method effectively captures the cumulative effect of multiple simultaneous variations when applied through the single variable partial differential framework to precisely capture uncertainty ($\bar{U}_i$). This technique offers a more holistic and precise estimation of the total uncertainty ($\bar{U}$), particularly in systems where interactions among variables are significant and cannot be ignored. In the present context, such a formulation not only reduces computational complexity but also enhances the interpretability of results. By breaking down how each variable contributes to the overall uncertainty, practitioners can better identify, isolate, and manage sources of error, inevitably improving the robustness and reliability of the system or model under risk analysis as shown in Equation 29.

$$\bar{U} = \pm\left[\frac{\partial(\beta)}{\partial(p)}\right] * \{p_m\} \quad (29)$$

where: $\bar{U}$ and β have already been addressed, and p_m indicates mean percent variation.

Equation 29 yields an uncertainty value ($\bar{U}$) of ±4.3%, which at first glance appears relatively minor and within acceptable bounds, given that $\bar{U} \leq 5.0\%$ is typically considered low and acceptable in many engineering and scientific contexts. The determination of $\bar{U}$ in this case is predominantly influenced by a single parameter, p_m. As a result, the overall uncertainty assessment may be overly optimistic, as it overlooks the potential contributions of other sources of variability that were either excluded or optimized during model simplification. Relying heavily on a single variable can mask underlying sensitivities and interdependencies that may significantly impact the reliability of the model in real-world applications. Therefore, while the reported uncertainty appears small, it may represent the true risk or variability inherent in the system.

7. Results and discussions

Reinforced concrete (RC) piers are among the most vulnerable structural components during vehicle collisions, primarily due to their exposed locations and slender geometries. Despite their susceptibility, the criteria that define their optimal impact performance and structural resilience under such dynamic events remain insufficiently understood. This highlights a critical need to assess the resilience of existing infrastructure against vehicular impacts in terms of energy dissipation [31], to develop targeted strategies that minimize damage and enhance performance.

This study presents a robust analytical framework for evaluating the material capacity and dynamic demand of RC pier, with an emphasis on their post-impact behavior. A detailed analytical model has been developed to quantify damage based on dynamic response characteristics. The model has been rigorously validated against commonly used multiple statistical approaches that were extracted from various published articles to predict post-impact severity. Results indicate that the proposed model consistently outperforms traditional methods, offering superior predictive accuracy, greater conservatism where necessary, and enhanced reliability under a range of impact conditions. Its performance demonstrates strong potential for practical implementation in both assessment and design applications, making it a valuable tool for improving the resilience of critical transportation infrastructure. The key findings from this investigation are summarized as follows:

- Performance-Based Assessment: The study investigates the dynamic response of RC piers subjected to short-duration, high-velocity impacts, offering a performance-based perspective that captures the severity of post-impact behavior and severity of damage in representative pier configurations.
- Material Demand and Model Correlation: This research explores material requirements essential for enhancing impact resistance. It establishes a meaningful and realistic correlation between the proposed mathematical model and other widely used statistical approaches, reinforcing the model's analytical rigor and predictive capability.
- High-Accuracy Prediction and Conservatism: Simulation results demonstrate high accuracy in estimating damage at both the pier and foundation levels under extreme vehicle impact scenarios. This instills P_f and corresponding β were evaluated across various utilized statistical models. The proposed model exhibits conservative stochastic behavior, whereas others tend to be more liberal, potentially underestimating risk.
- Uncertainty Quantification: The model underwent uncertainty analysis and yielded a coefficient of uncertainty ($\bar{U}$) of ±4.3%, which falls well within the acceptable threshold ($\bar{U} \leq 5\%$) for risk-sensitive applications. This makes the model a reliable tool for estimating post-impact damage without requiring destructive testing under extreme short duration dynamic loading conditions.
- Material Behavior and Calibration Insights: In addition to structural assessment, the study contributes valuable insights into material behavior and cognitive impact response, providing a robust foundation for improved decisive accurate future calibrations and material optimization strategies.
- The findings yield critical insights into material performance, energy dissipation mechanisms, and impact tolerance, thereby informing future calibration methodologies and advancing the development of structurally resilient and energy-efficient systems across diverse engineering applications by enhancing improved resilient structural designs.

8. Conclusions and future works

RC structural members including piers due to its non-deterministic behavior are among the most vulnerable components in vehicle collision scenarios, primarily due to their exposed locations, slender geometries and boundary conditions. Despite their critical role in supporting transportation infrastructure, the criteria defining their optimal impact performance and structural resilience under dynamic loading conditions remain insufficiently characterized. This gap underscores the pressing need to assess the capacity of existing RC piers to withstand vehicular impacts and to develop effective mitigation strategies that minimize damage while enhancing overall performance. The essence of this study is summarized as follows:

The proposed model, while conservative in nature, effectively captures the specific damage mechanisms associated with high-velocity vehicular impacts. It provides a cognitively robust framework that accounts for both risk and uncertainty in failure prediction, making it a reliable tool for post-impact assessment and resilience-based design.

By integrating damage quantification with probabilistic analysis, the model offers a comprehensive framework that balances deterministic accuracy with uncertainty management, making it suitable for risk-informed decision-making guideline.

The study introduces a cognitively driven approach to structural assessment, combining physical realism

with mathematical rigor to bridge the gap between theoretical prediction and practical implementation.

The model demonstrates strong agreement with simulation results and statistical benchmarks, validating its capacity to predict post-impact performance more accurately than commonly used empirical tools.

The model used can facilitate early detection and classification of damage severity without requiring destructive testing, thereby offering a cost-effective solution for evaluating existing infrastructure subjected to extreme impact events.

The uncertainty investigation reveals a narrow uncertainty band ($\bar{U}$ of ±4.3%), indicating high model reliability. This is particularly valuable in safety-critical assessments where prediction confidence is paramount.

Future research should focus on the rigorous experimental validation of the proposed mathematical model to establish its practical relevance and predictive reliability. While the analytical framework provides valuable theoretical insights into the mechanisms of cosmetic damage, it cannot be deemed complete without empirical confirmation. Experimental investigations are essential for assessing the model's behavior under real-world conditions, where variables are often interdependent and difficult to isolate. These studies should include controlled, high-precision testing across a diverse set of parameters, such as varying geometries, material compositions, loading rates, and impact conditions to capture the full spectrum of factors influencing cosmetic surface damage. By addressing these variables systematically, researchers can better evaluate the strengths and limitations of the model in representing complex structural responses.

Moreover, such validation efforts serve a dual purpose: enhancing the model's credibility and informing the development of more effective re-strengthening strategies. Understanding the nuances of how different systems behave under both operational and accidental stresses allows for tailored interventions that improve long-term durability and resilience. The integration of analytical modeling with empirical data is critical for transitioning theoretical concepts into practical engineering solutions. This holistic approach not only bridges the gap between simulation and application but also supports the design of structures that are better equipped to endure real-world challenges. Last but not the least, a well-validated model becomes a powerful tool for guiding maintenance protocols, improving safety standards with increased serviceability, and shaping future innovations in structural engineering.

Table 3 presents a comprehensive conversion chart designed to facilitate accurate translation between U.S. Customary Units and the International System of Units (SI). As a critical reference tool, the chart ensures precision and consistency in unit conversions, thereby supporting uniformity in calculations and analytical procedures throughout the study. By providing reliable and standardized conversion factors, it enables seamless cross-referencing and comparison of data across different measurement systems, enhancing both the clarity and the practical applicability of the presented results of all domains.

Table 3 Conversion of the US Customary Units to the Equivalent SI Units.

US Customary	SI
1 ksi	6.89 MPa (kN/mm^2)
1 ksi	6894.76 kN/m^2
1 kip-in	0.113 kN-m
1 kip	4.45 kN
1 lbs	0.00445 kN
1 mph	1.61 km/hr
1 ft-lb/sec	0.00136 kN-m/sec (1.36 N-m/sec)
1 in	0.0254 m (25.4 mm)
1 in^2	6.4516 cm^2
1 foot	30.48 cm

Nomenclature

I_{dyn}	dynamic impact force
I_r	peak reflected pressure or overpressure
t	duration of the impact event
E	kinetic energy absorbed by the impacted pier during the collision
I	moment of inertia of the pier's cross-section
L	length of the pier,
a	vertical distance from the base of the pier to the point where the impact occurs
b	vertical distance from the top of the pier to the impact point
c	perpendicular distance from the NA of the cross-section to the farthest extreme fiber
M	vehicle weight involved in the collision
k	stiffness of the vehicle's front structure
V_c	shear strength carried by the concrete and

V_s	transverse shear capacity
A_g	gross cross-sectional area of the concrete in the pier
A_s	total cross-sectional area of longitudinal steel
ŝ	shear span
N_{design}	design axial capacity of the pier
D	diameter of the pier cross-section
f_c'	28-day compressive strength of concrete
f_y	yield strength of main (longitudinal) reinforcing steel
A_h	area of a single hoop or spiral
D′	spiral or hoop diameter
S	pitch of the helix
σ_{yh}	yield stress of transverse steel
έ	strain rate of reinforcing steel
ξ	a constant depends on the dynamic yield stress of steel at the strain hardening zone
σ_{dyn}	yield stress of main reinforcing steel bar
ε^{eff}	equivalent plastic strain
E_p	plastic hardening modulus
β	hardening parameter
C & P	strain rate parameters
P_f	probability of failure,
λ	damage index
g(x)	limit state function and
x_i	vector of all the random variables included in the limit state function
p(a)	i^{th} of damage index (λ_i)
$P_D(a)$	logarithmic distribution of damage index
Φ	CDF of the standard normal random variable
Φ^{-1}	inverse of the tail probability function of the standard normal distribution
Δ	Allen's variables
Δ_E	energy as 0.25
Δ_S	space as 0.25,
Δ_I	impact as 0.25
Δ_{PC}	probability as 0.6
β_{model}	reliability index of model
β_{normal}	reliability index at normal distribution
β_{Nowak}	reliability index using Nowak's method
β_{Allen}	reliability index using Allen's method
$\beta_{standardized\ (Allen)}$	reliability index using standardized Allen's method

Acknowledgments

Funding to support this research was provided by Utah State University, Logan, Utah, USA, through its Research and Innovative Technology Administration and Department of Civil and Environmental Engineering.

Funding

This research is funded by the Department of Civil and Environmental Engineering, Utah State University, Logan, Utah, 84322, USA.

Competing Interests

The authors declare that there is no competing of interests.

Data Availability Statement

Some or all data, models, or code that support the findings of this study are available from the corresponding author upon reasonable request.

References

1. Harik IE, Shaaban AM, Gesund H, Valli G, Wang S. United States bridge failures, 1951–1988. Journal of Performance of Constructed Facilities. 1990;4(4):272–277.
2. Yu X, Chen Y, He Y. Vulnerability Assessment of Reinforced Concrete Piers Under Vehicle Collision Considering the Influence of Uncertainty. Buildings. 2025;15(8):1222.
3. Demartino C, Wu J, Xiao Y. Experimental and numerical study on the behavior of circular RC columns under impact loading. Procedia Engineering. 2017;199:2457–2462.

4. Roy S, Unobe I, Sorensen A. Vehicle-impact damage of reinforced concrete bridge piers: a state-of-the art review. Journal of Performance of Constructed Facilities. 2021;35(5):03121001.
5. Li R, Zhou D, Wu H. Experimental and numerical study on impact resistance of RC bridge piers under lateral impact loading. Engineering failure analysis. 2020;109:104319.
6. Zhou D, Li R. Damage assessment of bridge piers subjected to vehicle collision. Advances in structural engineering. 2018;21(15):2270–2281.
7. Buth CE BM, Williams WF, Fry GT. Collision loads on bridge piers: phase 2, report of guidelines for designing bridge piers and abutments for vehicle collisions. Austin, TX: Texas A&M Transportation Institute; 2011. [No. FHWA/TX–11/19–4973–4972]. Available from: https://rosap.ntl.bts.gov/view/dot/18684/dot_18684_DS1.xls.
8. Zhou D, Li R, Wang J, Guo C. Study on impact behavior and impact force of bridge pier subjected to vehicle collision. Shock and Vibration. 2017;2017(1):7085392.
9. Mestrovic D, Cizmar D, Miculinic L. Reliability of concrete columns under vehicle impact. Journal of WIT Transactions on the Built Environment. 2008;98:157–165.
10. Vrouwenvelder T. Stochastic modelling of extreme action events in structural engineering. Probabilistic Engineering Mechanics. 2000;15(1):109–117.
11. Roy S, Unobe ID, Sorensen AD. Reliability assessment and sensitivity analysis of vehicle impacted reinforced concrete circular bridge piers. Structures. 2022;37:600–612.
12. Roy S, Unobe ID, Sorensen A. Damage characterization and resilience optimization of reinforced concrete bridge piers under vehicle impact. Advances in bridge engineering. 2022;3(1):16.
13. Ni P, Li J, Hao H. Reliability analysis of bridges under different loads using polynomial chaos and subset simulation. Earthquake Engineering and Resilience. 2023;2(2):163–179.
14. Roy S. Approximate Performance Assessment of Composite Connector at High Velocity Vehicle Impact. International Journal of Scientific Research and Engineering Developmen. 2024;7:136–147.
15. Roy S. Reliability, sustainability, resiliency, and performance investigation of an embedded splice-sleeve connector at high velocity semi-trailer impact. Mechanical Engineering Advances. 2024;2(2):1633–1633.
16. AASHTO. AASHTO LRFD Bridge Design Specifications. 9th Edition [Internet]. American Association of State Highway and Transportation Officials; 2020. Available from: https://www.scirp.org/reference/referencespapers?referenceid=4020110.
17. Canadian Standards Association. Design of Highway Bridges. 1988. Report No.: CAN/CSA-S6-88.
18. MacGregor J, Wight JK, Teng S, and Irawan P. Reinforced concrete: Mechanics and design. Upper Saddle River, NJ: Prentice Hall; 2012.
19. Roy S. Reliability analysis and uncertainty evaluation for assessing low velocity car impacted cosmetic damage of prototyped RC bridge pier. Insight-Civil Engineering. 2024;7(1):623–623.
20. Roy S. A Study to Assess Residual Strength and Reliability Evaluation of Vehicle-Impacted Traditional Prototype RC Bridge Pier. Journal of Structural Design and Construction Practice. 2025;30(4):04025094.
21. Roy S. Sustainability and Resiliency Investigation of Grouted Coupler Embedded in RC ABC Bridge Pier at Vehicle Impact. Engineering and Applied Sciences. 2024;9:14–33.
22. Mander JB, Priestley MJ, Park R. Theoretical stress-strain model for confined concrete. Journal of structural engineering. 1988;114(8):1804–1826.
23. Feyerabend M. Hard transverse impacts on steel beams and reinforced concrete beams. University of Karlsruhe (TH), Germany. 1988. DOI: 10.1016/j.ijimpeng.2010.06.003.
24. Pantelides CP, Duffin JB, Reaveley LD. Seismic strengthening of reinforced-concrete multicolumn bridge piers. Earthquake Spectra. 2007;23(3):635–664.
25. Nowak AS, Collins KR. Reliability of structures. London, UK: CRC press; 2012.
26. Navidi WC. Statistics for engineers and scientists. New York, NY: McGraw-Hill; 2006.
27. Ayyub BM, McCuen RH. Probability, statistics, and reliability for engineers and scientists. 3rd ed. Boca Raton, FL: CRC press; 2016.
28. Huang C, Lin K, editors. A method for reliability assessment of aircraft structures subject to accidental damage. Proceedings of the 46th AIAA/ASME/ASCE/AHS/ASC Structures, Structural Dynamics and Materials Conference; 2005 April 18–21; Austin, TX, USA. Reston, VA: American Institute of Aeronautics and Astronautics.
29. Efthymiopoulos A, Goula A. Measuring the reliability and validity of Allen and Meyer's Organizational Commitment Scale in the Public Sector. Corporate Governance and Organizational Behavior Review. 2024;8(2):113–123.
30. Holman JP. Experimental methods for engineers. 6th ed: McGraw-Hill; 1994.
31. Roy S. Precision Assessment of Reinforced Concrete Pier Resilience Under High-Velocity Vehicle Impact Using an Energy-Based Analytical Model. International Journal of Bridge Engineering, Management and Research. 2025;2(3):214250027–214250021:214250019. DOI: 10.70465/ber.v2i3.40.